ChemComm

COMMUNICATION

View Article Online
View Journal | View Issue

Cite this: *Chem. Commun.*, 2026, **62**, 4601

Received 22nd January 2026,
Accepted 31st January 2026

DOI: 10.1039/d6cc00415f

rsc.li/chemcomm

A pyrene-4,5,9,10-tetraone/graphene composite film as a sustainable cathode material for aqueous iron-ion batteries

Wenwen Deng,†[ab] Ning Zhang,†[c] Ying Zhou,[b] Yuanyuan Quan,[b] Lei Yao,[b] Chengyang Zhang,[b] Yongxin Huang*[c] and Zhong Jin*[a]

A free-standing PTO/graphene composite cathode is developed for aqueous iron-ion batteries, enabling a reversible Fe^{2+} coordination storage mechanism. The battery exhibits stable cycling performance and good pouch-cell feasibility, offering a sustainable and environmentally friendly strategy for next-generation iron-based energy storage systems.

The transition toward a green and low-carbon society necessitates the development of environmentally benign, cost-effective, and sustainable electrochemical energy storage technologies.[1] Among various alternatives, aqueous metal-ion batteries (AMIBs) have garnered increasing attention due to their inherent safety, use of non-flammable electrolytes, and low production costs.[2–4] In particular, aqueous iron-ion batteries (AIIBs), which employ iron as the active anode material, offer remarkable advantages in terms of sustainability and economic feasibility due to the abundance of iron on Earth, its low toxicity, and its low cost.[5] With a high theoretical specific capacity of 960 mAh g^{-1} and a low redox potential (−0.44 V *vs.* SHE), iron is capable of suppressing parasitic hydrogen evolution, providing a favorable platform for constructing safe and stable aqueous energy storage systems.[6]

Despite these advantages, the development of suitable cathode materials remains a significant challenge that restricts the practical application of AIIBs. To date, research efforts have primarily focused on transition metal-based compounds such as layered vanadium oxides (*e.g.*, $VOPO_4{\cdot}2H_2O$, V_2O_5) and phosphate analogs.[7–11] These materials exhibit moderate capacity through reversible Fe^{2+} insertion/extraction. However, issues such as structural instability in aqueous electrolytes, transition metal dissolution, and environmental toxicity limit their long-term cycling stability and sustainability. Moreover, the non-renewable nature of transition metal resources further undermines their feasibility for large-scale applications.

Conductive polymers, such as polyaniline (PANI), represent another class of candidate materials for aqueous iron-organic battery systems due to their flexibility and high conductivity.[12] These systems demonstrate excellent rate capability and cycling performance. Nevertheless, their energy storage mechanism relies on the redox interaction between the electrode and anions in the electrolyte (*e.g.*, TOF^-), rather than on Fe^{2+} intercalation. This results in continuous electrolyte consumption during cycling, compromising the system's long-term stability and reversibility. Therefore, from both a mechanistic and environmental standpoint, such systems may not constitute ideal long-term solutions.

To address these limitations, we propose a novel aqueous iron-ion battery system based on pyrene-4,5,9,10-tetraone (PTO), a conjugated organic molecule featuring a rigid planar structure and four carbonyl functional groups.[13] PTO enables a genuine cation intercalation mechanism *via* reversible coordination with Fe^{2+} ions, without relying on anion participation. The material consists solely of C, H, and O elements, is free from heavy metals, and can be synthesized from abundant organic precursors, making it inherently green and sustainable. Additionally, PTO was combined with graphene (Gr) to form a dense electrode structure with enhanced electronic conductivity. The resulting binder-free composite electrode contains more than 99% active material and demonstrates enhanced energy utilization.

Electrochemical tests reveal that the PTO/graphene cathode delivers a specific capacity of 220 mAh g^{-1} at 0.1C (1C = 440 mAh g^{-1}) with 83.3% capacity retention over 200 cycles, indicating excellent reversibility of the Fe^{2+} intercalation/deintercalation process. *Ex situ* X-ray photoelectron spectroscopy

[a] *State Key Laboratory of Coordination Chemistry, MOE Key Laboratory of Mesoscopic Chemistry, MOE Key Laboratory of High Performance Polymer Materials and Technology, Jiangsu Key Laboratory of Green Energy Catalysis and Intelligent Chemical Engineering, Suzhou Key Laboratory of Green Intelligent Manufacturing of New Energy Materials and Devices, Tianchang New Materials and Energy Technologies Research Center, Institute of Green Chemistry and Engineering, School of Chemistry and Chemical Engineering, Nanjing University, Nanjing, Jiangsu 210023, China. E-mail: zhongjin@nju.edu.cn*

[b] *Beijing Key Laboratory of Environmental Science and Engineering, School of Material Science and Engineering, Beijing Institute of Technology, Beijing 100081, China*

[c] *School of Material Science and Engineering, Suzhou University of Science and Technology, Suzhou 215000, China. E-mail: huangyx@bit.edu.cn*

† These authors contributed equally to this work.

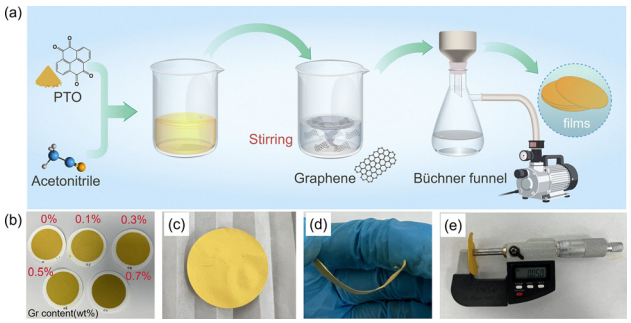

Fig. 1 (a) Schematic illustration of the fabrication process of PTO/Gr composite films. (b) Digital photographs of PTO/Gr composite films with different graphene contents (0–0.7 wt%). (c) Photograph of a free-standing PTO/Gr composite film. (d) Optical image demonstrating the good flexibility of the composite film. (e) Thickness measurement of the PTO/Gr (0.5 wt%) film.

(XPS) and X-ray diffraction (XRD) analyses were conducted at different charge/discharge states to elucidate the underlying reaction mechanism. Furthermore, the pouch-type battery was successfully assembled, showcasing its potential for future large-scale deployment. Our work offers a promising alternative to conventional inorganic and anion-insertion-based cathode materials. It addresses key limitations in environmental compatibility, resource sustainability, and electrochemical reversibility, providing a viable route toward developing safe, low-cost, and sustainable aqueous energy storage technologies.

Fig. 1 presents the fabrication procedure and physical characteristics of the PTO/graphene composite films. As illustrated in Fig. 1a, PTO was first dispersed in acetonitrile, followed by the introduction of graphene under continuous stirring to form a homogeneous suspension. The resulting mixture was then subjected to vacuum filtration using a Büchner funnel, enabling the formation of uniform composite films. Photographs of the obtained films with different graphene contents (0–0.7 wt%) are shown in Fig. 1b, where a gradual color deepening can be observed with increasing graphene loading, indicating the successful incorporation of graphene into the PTO matrix. A comparative analysis of the morphologies of PTO/Gr films prepared with different graphene contents in Fig. S1 reveals a pronounced dependence of film integrity on the graphene loading. The pristine PTO film, as well as samples with low graphene contents (0.1 and 0.3 wt% Gr), fail to form continuous and self-supporting membranes, exhibiting loose architectures and poor mechanical integrity. Upon increasing the graphene content to 0.5 wt%, a uniform, continuous, and densely packed PTO/Gr film is successfully obtained, indicating markedly enhanced film-forming ability and mechanical stability. Further increasing the graphene content to 0.7 wt% does not lead to an obvious improvement in the structural integrity of the resulting membrane.

Fig. S2a show that all samples with varying graphene contents (0, 0.3, 0.5, 0.7 wt%) display similar XRD peak positions, indicating the retention of PTO's crystalline structure upon graphene incorporation. The lack of peak shifts suggests that graphene is physically blended rather than intercalated into the PTO lattice. A slight reduction in peak intensity with increasing graphene content may result from decreased crystallinity or dilution effects due to the amorphous nature of graphene. Fig. S2b presents the FTIR spectra of the same samples. The consistent absorption bands for C=O (~1720 cm^{-1}), C=C (~1600 cm^{-1}), and C–C/C–O (1000–1300 cm^{-1}) confirm the preservation of PTO's functional groups. The absence of significant peak shifts and only minor intensity changes suggest that PTO exhibits structural stability and minimal chemical interaction with graphene.

Fig. 1c displays a digital photograph of the optimized PTO/Gr membrane, which exhibits a uniform appearance and good macroscopic integrity, confirming the successful formation of a self-supporting organic composite film. The membrane can be readily handled and transferred without fracture, indicating sufficient mechanical robustness. As shown in Fig. 1d, the PTO/Gr film maintains structural continuity under bending, demonstrating excellent flexibility and mechanical tolerance, which are essential for ensuring intimate interfacial contact during cell assembly. The cross-sectional image in Fig. 1e reveals a relatively uniform thickness of approximately 50 μm across the entire membrane, suggesting homogeneous film formation during the antisolvent-induced filtration process.

Fig. 2 shows the electrochemical performance of the Fe//PTO battery. As shown in Fig. 2a, the rate performance measured at stepwise increasing current densities of 0.1, 0.2, 0.4, 0.6, 0.8, 1, and 2C shows an initial discharge capacity of approximately 300 mAh g^{-1} at 0.1C, which gradually decreases to about 260, 230, 200, 170, 150, and 120 mAh g^{-1} as the current density increases, respectively. The PTO/Gr cathode exhibits a higher specific capacity than other representative cathode materials, including PANI, VO_2, and $VOPO_4{\cdot}2H_2O$. Detailed comparisons of the electrochemical performance are summarized in Table S1. The high specific capacity and excellent rate capability of the PTO/Gr electrode can be mainly attributed to the large inter-rod void spaces among the rod-like PTO particles, together with the

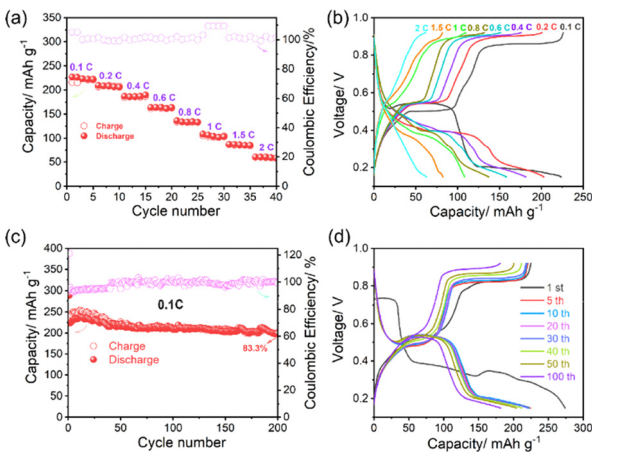

Fig. 2 Electrochemical performance of the PTO film electrode in an Fe ion battery. (a) Rate performance at various current densities ranging from 0.1 to 2C. (b) Galvanostatic charge–discharge voltage profiles collected at different C-rates. (c) Long-term cycling performance at 0.1C. (d) Representative charge–discharge voltage profiles at selected cycles (1st, 5th, 10th, 20th, 30th, 40th, 50th, and 100th).

homogeneous dispersion of graphene within the electrode matrix. This unique microstructural architecture establishes continuous and efficient pathways for both ion and electron transport, thereby markedly enhancing the electrochemical reaction kinetics. The corresponding galvanostatic charge–discharge profiles, collected at different current densities (Fig. 2b), reveal a gradual increase in polarization with increasing rate. Meanwhile, the characteristic discharge plateaus, centered at approximately 0.45–0.55 V, remain discernible even at 2C, demonstrating favorable reaction kinetics and preserved redox activity under high-rate operation. Long-term cycling at 0.1C (Fig. 2c) delivers an initial discharge capacity of approximately 260 mAh g^{-1}. It retains 8–217 mAh g^{-1} after 200 cycles, corresponding to a capacity retention of 83.3%, indicative of highly reversible electrochemical processes and effectively suppressed parasitic reactions. Representative charge–discharge voltage profiles recorded at selected cycle numbers (1st, 5th, 10th, 20th, 30th, 40th, 50th, and 100th cycles) exhibit nearly overlapping curves with negligible voltage hysteresis growth (Fig. 2d), confirming minimal polarization increase during prolonged cycling and highlighting the excellent interfacial stability and structural integrity of the electrode upon repeated charge–discharge.

The reversible Fe^{2+} storage mechanism of PTO was systematically investigated by combining XPS, *ex situ* XRD, and schematic analysis (Fig. 3). As revealed by the high-resolution C 1s XPS spectra (Fig. 3a), the pristine PTO electrode exhibits characteristic contributions from C–C/C═C and C═O species, originating from the conjugated aromatic framework and carbonyl groups, respectively. Upon full discharge, a pronounced decrease in the C═O component is observed, accompanied by the emergence of a distinct C–O signal, indicating the electrochemical reduction of carbonyl groups and the formation of Fe–O coordination bonds during Fe^{2+} insertion. Meanwhile, the noticeable broadening and redistribution of the C═C-related peaks suggest electron delocalization within the π-conjugated system induced by Fe^{2+} coordination. Importantly, these spectral features are largely restored after subsequent charging, with the C–O contribution diminishing and the C═O signal recovering to a level comparable to that of the pristine state, demonstrating the highly reversible nature of the carbonyl redox chemistry. Consistently, *ex situ* XRD patterns (Fig. 3b) further corroborate this reversible structural evolution. While the pristine PTO shows well-defined diffraction peaks characteristic of its crystalline framework, additional reflections appear fully discharged, which can be assigned to the formation of an Fe-inserted PTO phase. These newly emerged peaks disappear upon recharging, and the diffraction profile nearly returns to its original form, indicating that Fe^{2+} insertion induces a reversible phase transformation rather than irreversible lattice degradation. Based on these observations, a reversible two-electron Fe^{2+} storage mechanism is proposed (Fig. 3c), in which the carbonyl groups act as the primary redox-active sites, enabling reversible Fe^{2+} coordination/decoordination during the discharge and charge processes. Such a coordination-driven redox mechanism endows PTO with both structural reversibility and stable electrochemical activity, thereby underpinning its feasibility as an organic cathode material for aqueous iron-ion batteries.

Fig. 4 presents the electrochemical performance of a pouch-type iron-ion battery, with the inset showing the photograph of the assembled pouch cell. As illustrated in Fig. 4a, the galvanostatic charge–discharge profiles recorded at a current density of 50 mA g^{-1} for the 1st, 5th, and 10th cycles exhibit well-defined and nearly overlapping voltage plateaus in the range of approximately 0.4–0.6 V. Notably, only negligible polarization evolution is observed upon repeated cycling, indicating highly reversible Fe^{2+} redox reactions and stable reaction kinetics in the pouch-cell configuration. The corresponding cycling performance (Fig. 4b) delivers an initial discharge capacity of about 170–180 mAh g^{-1}, which gradually stabilizes at approximately 135–140 mAh g^{-1} after 100 cycles, corresponding to a capacity retention of around 80%. Meanwhile, a consistently high coulombic efficiency close to 100% is maintained throughout the entire cycling process, further confirming the excellent reversibility of the iron-ion storage chemistry. Collectively, these results demonstrate the robust cycling stability and high electrochemical reversibility of the pouch-type iron-ion battery, highlighting the effective translation of iron-ion battery chemistry from laboratory-scale cells to practical pouch-cell configurations, as well as its promising potential for future development, practical feasibility, and scalable aqueous energy storage applications.

In conclusion, a pyrene-4,5,9,10-tetraone/graphene (PTO/Gr) composite cathode has been demonstrated as an efficient and sustainable organic host for aqueous iron-ion batteries. The

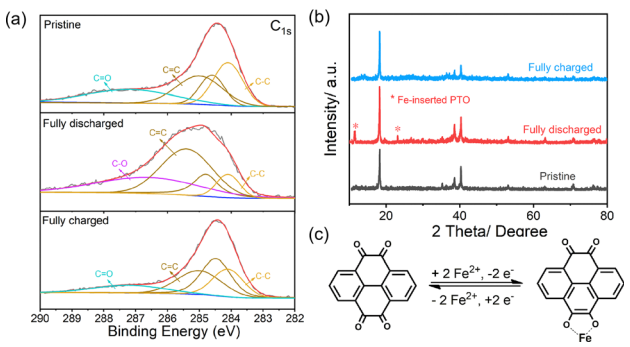

Fig. 3 (a) High-resolution C 1s XPS spectra of PTO electrodes in pristine, fully discharged, and fully charged states. (b) *Ex situ* XRD patterns of PTO at different electrochemical states. (c) Schematic illustration of the reversible Fe^{2+}-storage mechanism in PTO involving a two-electron redox process.

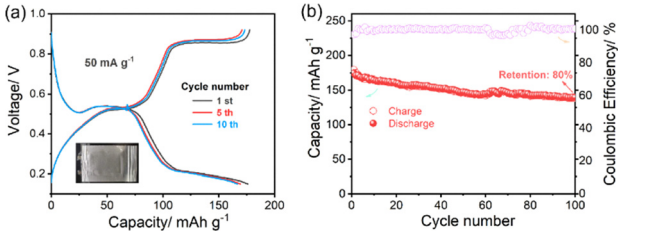

Fig. 4 (a) Galvanostatic charge–discharge voltage profiles of the Fe//PTO-film pouch cell at a current density of 50 mA g^{-1} for the 1st, 5th, and 10th cycles. (b) Cycling performance and corresponding coulombic efficiency of the electrode over 100 cycles at 50 mA g^{-1}.

PTO molecule enables a genuine and reversible Fe^{2+} coordination storage mechanism through carbonyl redox chemistry. At the same time, the incorporation of graphene ensures sufficient electronic conductivity and mechanical integrity of the free-standing electrode. The resulting battery exhibits stable cycling performance and reliable pouch-cell operation. This work provides a proof-of-concept strategy for constructing environmentally benign organic cathodes for aqueous multivalent-ion energy storage systems.

Conflicts of interest

There are no conflicts to declare.

Data availability

The authors confirm that the data supporting the findings of this study are available within the article and its supplementary information (SI), which includes detailed experimental procedures, materials synthesis, characterization data, electrochemical measurements, and additional figures and tables. Supplementary information is available. See DOI: https://doi.org/10.1039/d6cc00415f.

Acknowledgements

This work was funded by The Natural Science Foundation of the National Natural Science Foundation of China (U25A20628, 22561160129, 22479074, and 22475096), the Jiangsu Higher Education Institutions of China (23KJB150032 and 24KJA15004), the Equipment Pre-Research and Ministry of Education Joint Fund (8091B02052407), the Fundamental Research Program Key Project of Jiangsu Province (BK20253008), the Natural Science Foundation of Jiangsu Province (BK20240400 and BK20241236), the Science and Technology Major Project of Jiangsu Province (BG2024013), the Scientific and Technological Achievements Transformation Special Fund of Jiangsu Province (BA2023037), the Academic Degree and Postgraduate Education Reforming Project of Jiangsu Province (JGKT24_C001), the Key Core Technology Open Competition Project of Suzhou City (SYG2024122), the Open Research Fund of Suzhou Laboratory (SZLAB-1308-2024-TS005), and the Chenzhou National Sustainable Development Agenda Innovation Demonstration Zone Provincial Special Project (2023sfq11).

References

1 W. Zhao, S. J. B. Rubio, Y. Dang and S. L. Suib, *ACS EST Eng.*, 2022, **2**, 20–42.
2 W. Deng, Y. Shen, J. Qian and H. Yang, *Chem. Commun.*, 2015, **51**, 5097–5099.
3 S. Wang, N. Hu, Y. Huang and W. Deng, *Appl. Surf. Sci.*, 2023, **619**, 156725.
4 J. Wang, X. Zhang, Z. Yan, Z. Rui, Z. Yang, Y. Huang and W. Deng, *Chem. Eng. J.*, 2023, **459**, 141649.
5 J. K. Yadav, B. Rani, P. Saini and A. Dixit, *Energy Adv.*, 2024, **3**, 927–944.
6 H. Luo, X. Su, Z. Chen, H. Guo, R. Zhao, Q. Gao, M. Lu and T. Liu, *Adv. Mater.*, 2025, **37**, 2507978.
7 Y. Xu, X. Wu, S. K. Sandstrom, J. J. Hong, H. Jiang, X. Chen and X. Ji, *Adv. Mater.*, 2021, **33**, 2105234.
8 X. Guo, C. Li, W. Deng, Y. Zhou, Y. Chen, Y. Xu and R. Li, *Chin. Chem. Lett.*, 2025, **36**, 109715.
9 C. Li, Y. Xu, W. Deng, Y. Zhou, X. Guo, Y. Chen and R. Li, *Small*, 2024, **20**, 2305766.
10 Z. He, G. Wang, R. Yu, Y. Jiang, M. Huang, F. Xiong, S. Tan, M. F. L. De Volder, Q. An and L. Mai, *ACS Nano*, 2024, **18**, 17304–17313.
11 Y. Xu, C. Li, W. Deng, J. Zhu, Y. Zhou, R. Zhu, C. Huang, W. Zou and R. Li, *Chem. Commun.*, 2023, **59**, 8576–8579.
12 H. Lv, Z. Wei, C. Han, X. Yang, Z. Tang, Y. Zhang, C. Zhi and H. Li, *Nat. Commun.*, 2023, **14**, 3117.
13 Z. Guo, Y. Ma, X. Dong, J. Huang, Y. Wang and Y. Xia, *Angew. Chem., Int. Ed.*, 2018, **57**, 11737–11741.

